Available online at www.sciencedirect.com
ScienceDirect
Journal of the European Ceramic Society 28 (2008) 1161–1167
www.elsevier.com/locate/jeurceramsoc

Thermal stability of ordered mesoporous yttria-stabilized zirconia

I-Ming Hung [a,*], Kuan-Zong Fung [b,1], De-Tsai Hung [b,1], Min-Hsiung Hon [b,1]

[a] *Yuan Ze Fuel Cell Center, Department of Chemical Engineering and Materials Science, Yuan Ze University, No. 135, Yuan-Tung Road, Chungli, Taoyuan 320, Taiwan*

[b] *Department of Materials Science and Engineering, National Cheng Kung University, No. 1, Dashiue Road, Tainan 701, Taiwan*

Received 4 May 2007; received in revised form 31 August 2007; accepted 10 September 2007
Available online 19 November 2007

Abstract

The hexagonal mesostructured nanocrystalline 16 mol% yttria-stabilized zirconia (8YSZ) formed by using a Pluronic triblock copolymer F127 as template is reported as a function of temperature. The characterization of the samples is achieved using wide-angle XRD diffraction, small-angle XRD diffraction, nitrogen adsorption–desorption, and transmission electron microscopy. The mesostructured 8YSZ calcined at 500 °C is found to be based upon a 2D periodic array of mesopores with diameter around 6.4 nm and the 8YSZ framework is composed of about 4.8 nm nanocrystallites. The sample has a BET surface area of 124 m^2/g with a narrow pore size distribution. The ordered mesoporous structure remained even after calcination up to temperature of 600 °C grew out collapsed gradually when calcined above 700 °C owing to the fact that the crystallite size of 8YSZ larger than the inorganic pore-wall thickness.

Keywords: YSZ; ZrO_2; Calcination; Grain size; Porosity; Mesoporous structure

1. Introduction

Since the successful preparation of ordered mesoporous silica by scientists in Mobil Corp., the synthesis methods and applications for amorphous silica-based mesoporous materials have been described in detail in several excellent reviews.[1–3] In recent years, the preparation of mesoporous metal oxides has also been documented because they have great potential in a wide range of applications, such as photovoltaics, biochemicals, the lithium-ion battery, the solid oxide fuel cell (SOFC), and sensors.[4–9] However, the difficulties of handling mesoporous metal oxides, in part due to the variable valence, coordination number, and high hydrolysis/condensation reactivity, led to the slow development in this field. Pinnavaia and co-workers[10] clearly show that there is a displacement mechanism caused by non-ionic micellar aggregates resulting in wormlike surfactant micelles structure. Most mesoporous transition metal (TM) oxides are less regular than those in mesoporous silica-based materials (as determined by small-angle XRD and TEM), but still exhibit high specific surface areas and narrow pore size distributions.

Yttria-stabilized zirconia (YSZ) is an important functional oxide for many structural and electronic applications, such as solid oxide fuel cells (SOFCs), gas sensors, automotive exhaust three-way catalysts substrates and membranes due to its excellent chemical resistance, refractory character, oxygen ionic conductivity and polymorphous nature.[11–15] For the above applications, mesoporous YSZ with large surface area, high porosity and nanocrystallinity is highly favorable. Different synthetic strategies have been developed using a variety of templates. Ozin and co-workers[16] were first to extend the supramolecular template approach to the synthesis of mesoporous 8YSZ using cetyltrimethylammonium bromide ($[CH_3(CH_2)_{15}N^+(CH_3)_3Br^-]$, CTAB) as the template and using a glycolate-modified inorganic solution as the metal ion precursor. Chen and Liu[17] reported the preparation of 8YSZ/NiO using Pluronic P103 as a structure-directing agent and inorganic chlorides as precursors in a non-aqueous medium. Gedanken and co-workers[18] reported that mesoporous 8YSZ was obtained when octanoic acid ($C_7H_{15}COOH$) was used as a templating agent and Zr(*i*-OPr)$_4$ and Y_2O_3 were used as metal ion sources. However, these mesoporous 8YSZ materials

* Corresponding author. Tel.: +886 3 4638800x2569; fax: +886 3 4630634.
E-mail addresses: imhung@saturn.yzu.edu.tw (I.-M. Hung), kzfung@mail.ncku.edu.tw (K.-Z. Fung).
[1] Tel.: +886 6 2757575x62903; fax: +886 6 2380208.

0955-2219/$ – see front matter © 2007 Elsevier Ltd. All rights reserved.
doi:10.1016/j.jeurceramsoc.2007.09.044

consisted of crystallized particles in a wormhole-like mesoporous structure. A periodically organized hexagonal/cubic mesoporous 20 mol% yttria-stabilized zirconia (10YSZ) with crystallized walls was first developed by Soler-Illia and coworkers.[19] The crystallinity and crystallite size of mesoporous YSZ in the pore-wall are very important because both the potential applications and the periodicity of the mesoporous structure rely on the intrinsic properties of YSZ governed by the nature of its crystalline phase and crystallite size.

Herein, we report the reproducible synthesis of cubic 8YSZ presenting a periodically organized 2D hexagonal mesoporous structure with high surface area associated with nanocrystalline inorganic walls. In addition, the relation between the ordered mesoporous structure and the crystallite size of 8YSZ calcined between 500 and 800 °C was investigated by small-angle X-ray diffraction (SAXD) in conjunction with high-resolution transmission electron microscopy (HR-TEM).

2. Experimental

The ordered mesoporous 8YSZ was prepared by evaporation-induced self-assembly (EISA).[20] The molar ratio of Y/(Y + Zr) was 0.148. In a typical synthesis, 0.0644 mole of zirconium chloride (99.9%, Alfa) and 0.0112 mole yttrium chloride (99.5%, Alfa) were added to the surfactant ethanol solution where 4.49 g of poly(alkylene oxide) block copolymer Pluronic F127 ($EO_{106}PO_{70}EO_{106}$) (where EO is ethylene oxide and PO is propylene oxide) was dissolved in 140 g of ethanol (EtOH). Water was added to this mixture solution (molar ratio of H_2O/metal is 20), which result in a very acidic solution to prevent precipitation. The solutions contain 1(Y + Zr):0.0047 F127:40 EtOH:20 H_2O. The resulting sol solution was gelled in an open Petri dish and underwent solvent evaporation at RH = 40% at 40 °C for 3 days. The as-made bulk samples were heat treated at 500 – 800 °C for 4 h with a heating rate of 1 °C/min.

Small-angle X-ray diffraction was performed on the beam line 17A at the National Synchrotron Radiation Research Center (NSRRC) in Taiwan operated at an energy of 9.3 keV (λ = 1.33320 Å). The phase identification was performed by wide-angle XRD using a Rigaku, Model Rad II diffractometer with Cu Kα radiation (λ = 1.5406 Å) and Ni filter, operated at 30 kV, 20 mA with scanning rate of 1°/min. The average crystallite size was calculated using Scherrer's equation from the (1 1 1) peak with scanning rate of 0.1°/min.[21] High-resolution transmission electron microscopy was performed using a FEI E.O Tecnai F20 G2 MAT S-TWIN Field Emission Gun Transmission Electron Microscope. The nitrogen adsorption and desorption isotherms were measured using a Micromeritics ASAP 2010 system at 77 K after the samples were vacuum-dried at 200 °C overnight.

3. Results and discussion

Fig. 1 shows the comparison of the wide-angle XRD patterns of the 8YSZ samples as-synthesized and as calcined at 500 – 800 °C. As expected, the structure of the as-synthesized sample is amorphous. The samples calcined at various temperatures indicate that mainly the cubic phase of 8YSZ was present, the peaks including the (1 1 1), (2 0 0), (2 2 0), (3 1 1), (2 2 2) and (4 0 0) reflections (JCPDS no. 82-1246). The lattice parameter *a* for all samples is about 5.17 Å. It should be noted that broad peaks corresponding to nanocrystalline 8YSZ in the pore-walls were observed upon calcination above 500 °C. The XRD peaks become more intense and narrow with increasing calcination temperature. The average crystallite size of 8YSZ samples calcined at 500 – 800 °C as calculated from the Scherrer's equation using the (1 1 1) diffraction peak of 8YSZ is shown in Table 1.

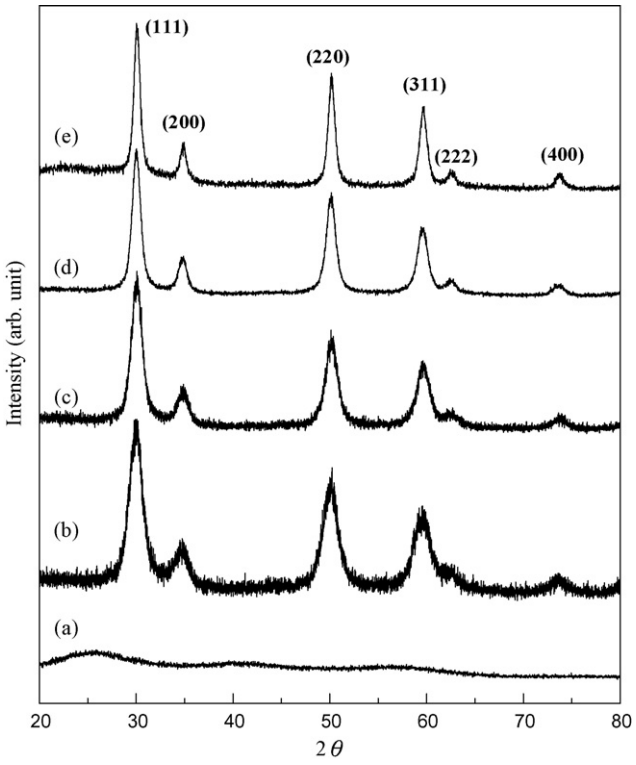

Fig. 1. XRD patterns of mesoporous 8YSZ (a) as-synthesized and calcined at (b) 500 °C, (c) 600 °C, (d) 700 °C, and (e) 800 °C for 4 h.

Energy dispersive X-ray spectroscopy (EDX) measurements (not shown here) reveal no detectable chloride ion, which is indicative of complete elimination of Cl^- upon calcination. The Y/(Y + Zr) mole ratio is 0.149 for the calcined samples, which corresponds well with the original stoichiometry of reactants during the synthesis (Y/(Y + Zr) = 0.148), and may be denoted as 8YSZ. The results of EDS and wide-angle XRD both indicated that the yttrium cation is well-dispersed in the zirconia matrix above 500 °C and consequently stabilized the cubic fluorite phase to room temperature.

Small-angle XRD patterns of as-synthesized precursor and calcined samples are shown in Fig. 2. The as-synthesized precursor (Fig. 2a) shows an intense well-defined peak at 0.37° of 2θ angle with *d* = 207 Å. Samples calcined at 500 and 600 °C present very high order arrangement (Fig. 2b and c). The 500 °C-calcined sample shows two well-resolved diffraction peaks, located at 0.62° and 1.09° 2θ angles with *d* = 123 and 70 Å. These two peaks display a *d*-value ratio of $1 : \sqrt{3}$, which can be assigned to (1 0 0) and (1 1 0) diffraction planes as is typically

Table 1
Specific surface area, pore size and crystallite size of samples calcined at various temperatures

Calcination temperature (°C)	S_{BET} (m^2/g)	BJH pore size (nm)	Pore size[a] (nm)	Pore-wall thickness[b] (nm)	Crystallite size[c] (nm)	Crystallite size[d] (nm)
500	124	6.4	6.9 ± 0.3	5.5 ± 0.3	4.8 ± 0.5	4.5 ± 0.6
600	90	6.3	7.1 ± 0.4	6.5 ± 0.5	6.4 ± 0.9	6.7 ± 0.4
700	60	11.1	–	–	8.3 ± 1.0	8.2 ± 0.5
800	29	18.4	–	–	16.6 ± 1.5	17.8 ± 1.0

[a] Pore size was observed by HR-TEM.
[b] Pore-wall thickness was observed by HR-TEM.
[c] Crystallite size was observed by HR-TEM.
[d] Crystallite size determined by XRD.

observed in the 2D hexagonal structure. The 600 °C-calcined sample shows only one diffraction peak, located at 0.65° 2θ angle with d_{100} = 118 Å. The lattice constant, a calculated from the d-spacing is 240 Å for the precursor, 142 and 136 Å for the samples calcined at 500 and 600 °C, respectively. It is suggested that the wall restructuring is accompanied by pore shrinkage during the template removal and higher calcination thermal treatment. The measured d_{100} spacing of the precursor is about 8% larger than that previously reported for hexagonal mesoporous 10YSZ using the same template, F127, and metal chlorides as the sources

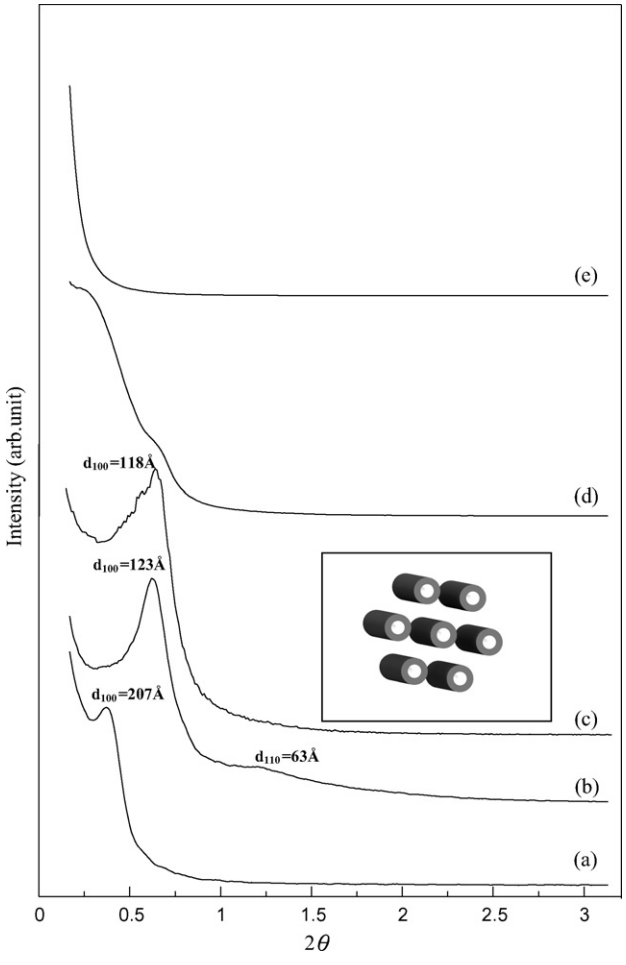

Fig. 2. SAXD patterns of mesoporous 8YSZ (a) precursor and calcined at (b) 500 °C, (c) 600 °C, (d) 700 °C, and (e) 800 °C for 4 h. The insert in part (c) is the schematic diagram for 2D hexagonal structure.

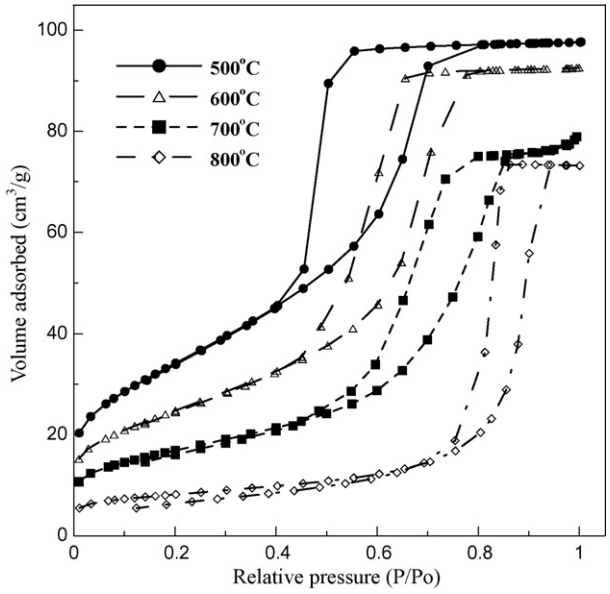

Fig. 3. Nitrogen adsorption–desorption isotherms of mesoporous 8YSZ calcined at various temperatures for 4 h.

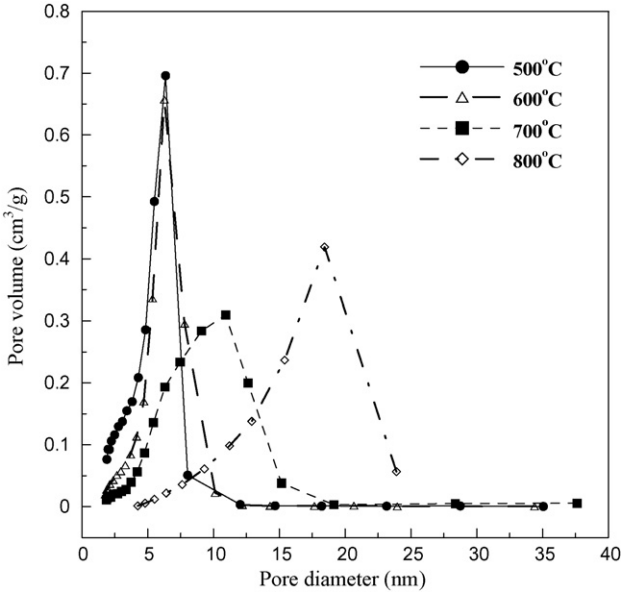

Fig. 4. BJH pore size distribution of mesoporous 8YSZ calcined at various temperatures for 4 h.

in the alcohol solution.[19] A large and repeated lattice usually contributes to the presence of reflections at small angles. The presence of these reflections suggests that these samples may consist of a highly regular or ordered structure. However, on close inspection it can be seen that only the most intense feature (1 0 0) can be observed. It is suggested that the pores do not perfectly parallel each other and that there is lack of directional uniformity over long length. In comparison to the data presented by Ozin and co-workers,[16] the small-angle XRD data shown in our text is of very high quality. A very broad and low intensity peak can be observed at 700 °C (Fig. 2d) located at 0.58° 2θ angle, which means that the ordered mesoporous structure collapsed gradually. As calcined at 800 °C (Fig. 2e), there is no peak observed on the small-angle XRD pattern. These results indicate that the mesoporous structure is completely lost above 800 °C.

Fig. 3 shows the nitrogen adsorption–desorption isotherms for the mesoporous 8YSZ calcined at various temperatures. The samples calcined at 500 and 600 °C exhibited a distinct large hysteresis loop from 0.4 to 0.8 of relative partial pressure (P/P_0). Such a behavior is the typical characteristic of mesoporous materials namely a type IV isotherm assigned to mesoporous structure. The nitrogen adsorption–desorption gives a BET specific surface area 124 m^2/g and a pore volume of 0.15 cm^3/g for

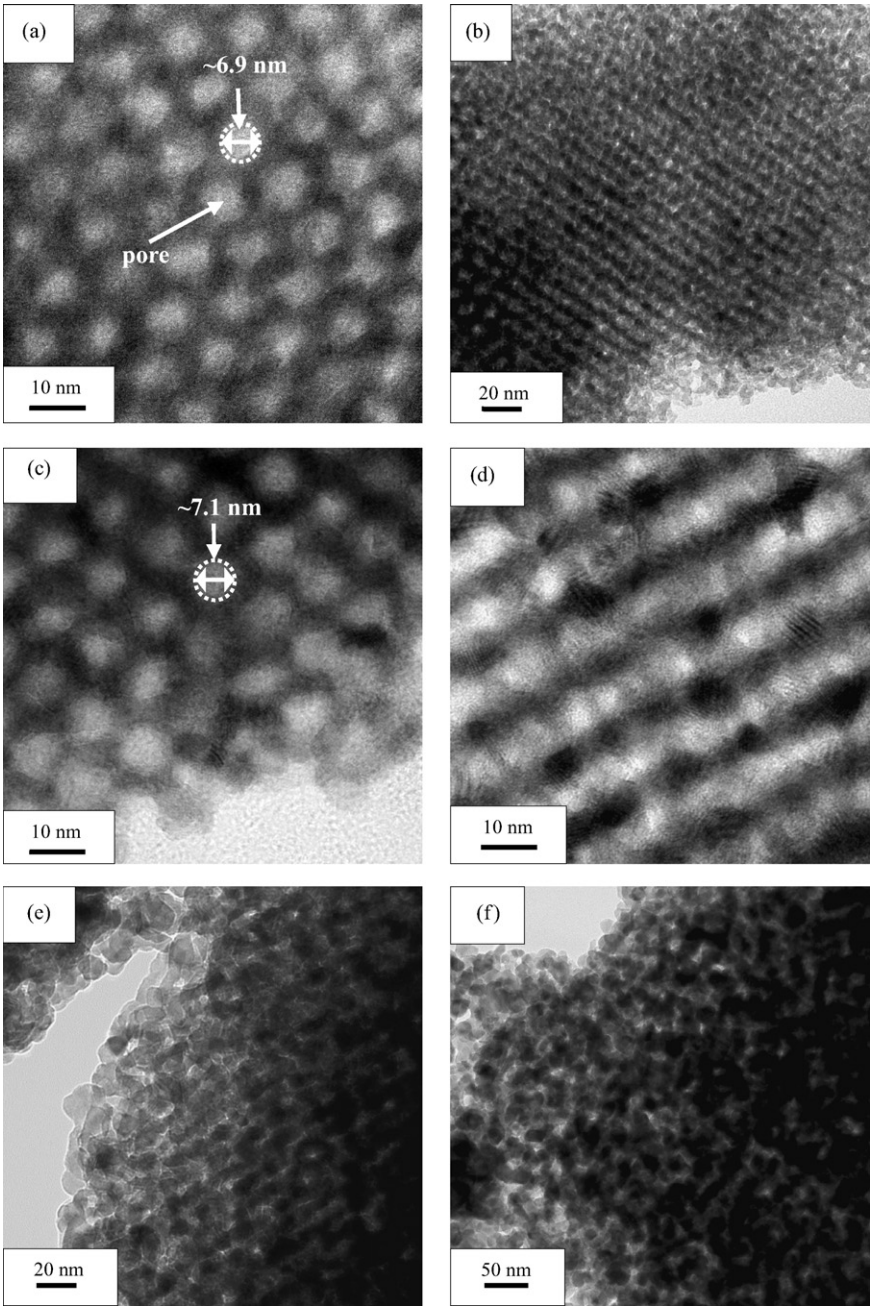

Fig. 5. TEM images of mesoporous 8YSZ calcined at (a and b) 500 °C, (c and d) 600 °C, (e) 700 °C, and (f) 800 °C for 4 h. The images are projections parallel to the following direction: (a and c) [1 0 0] and (b and d) [1 1 0].

the sample calcined at 500 °C and 90 m^2/g and a pore volume of 0.14 cm^3/g for the sample calcined at 600 °C. It was found that the hysteresis loop shifts to higher P/P_0 with increasing calcination temperature. As the calcined temperature increased to 800 °C, the sample shows a very poor isotherm, accompanied by a decreased in BET surface area of 75% from 124 to 29 m^2/g and a decrease in pore volume of 27% from 0.15 to 0.11 cm^3/g.

Fig. 4 shows the Barret-Joyner-Halenda (BJH) pore-size distribution for the mesoporous 8YSZ calcined at various temperatures. A BJH analysis indicates that the samples calcined at 500 and 600 °C exhibited rather narrow pore size distribution with the mean pore size being 6.4 and 6.3 nm, respectively, and the half-width at half-maximum intensity (FWHM) being 1.9 and 2.1 nm. The narrow pore size distribution implies that the samples have very regular pore channels in the mesoporous region. The samples calcined at 700 and 800 °C exhibited mean pore size of 11.1 and 18.4 nm and the FWHM is 6.0 and 6.2 nm, respectively. This result indicated that the arrangement of mesopores in the samples calcined at 700 and 800 °C is disordered.

TEM images of calcined 8YSZ powders shown in Fig. 5. Fig. 5(a)–(d) reveal a well-defined 2D hexagonal mesoporous structure along the (1 0 0) and (1 1 0) plane in the samples calcined at 500 and 600 °C from which all of the surfactant had been removed. They were arranged in arrays and exhibit regular long-range ordered patterns in large domains, which is consistent with the result from SAXD. Numerous highly ordered pores have mean pore size of ~6.9 and 7.1 nm for 500 and 600 °C-calcined samples that nicely match the BJH pore size analyses. In the sample calcined at 700 °C (Fig. 5(e)), the pores do not parallel consistent each other well and the ordered mesoporous structure has gradually collapsed with the result of small-angle XRD in Fig. 2 (d), which shows a broad and low intensity peak. Only aggregated and sintered nano-particles were observed and most of the ordered arrangement of the mesopores has been lost, but the porosity is still present in the sample calcined at 800 °C.

In order to take a closer look at the microstructure and crystal size of the mesoporous 8YSZ calcined at various temperatures, HR-TEM investigations are provided as shown in Fig. 6. It can be observed that the calcined samples are totally composed of highly ordered 8YSZ nanocrystallites. A fully crystallized 8YSZ framework with orderly arranged mesopores connecting in between was clearly observed for the samples calcined at 500 and 600 °C. Clear lattice images along the various directions were clearly observed. The crystallite size of 8YSZ samples calcined at various temperatures measured from HR-TEM is shown in Table 1. It was found that the crystal size of mesoporous 8YSZ measured from HR-TEM is consistent with the data calculated from XRD. The sizes of the calcined at 500 and 600 °C are in the range of 4.8 – 6.4 nm, which is smaller than the thickness of the pore-walls (~6.5 nm). The nanocrystallites do not significantly grow as the calcination temperature

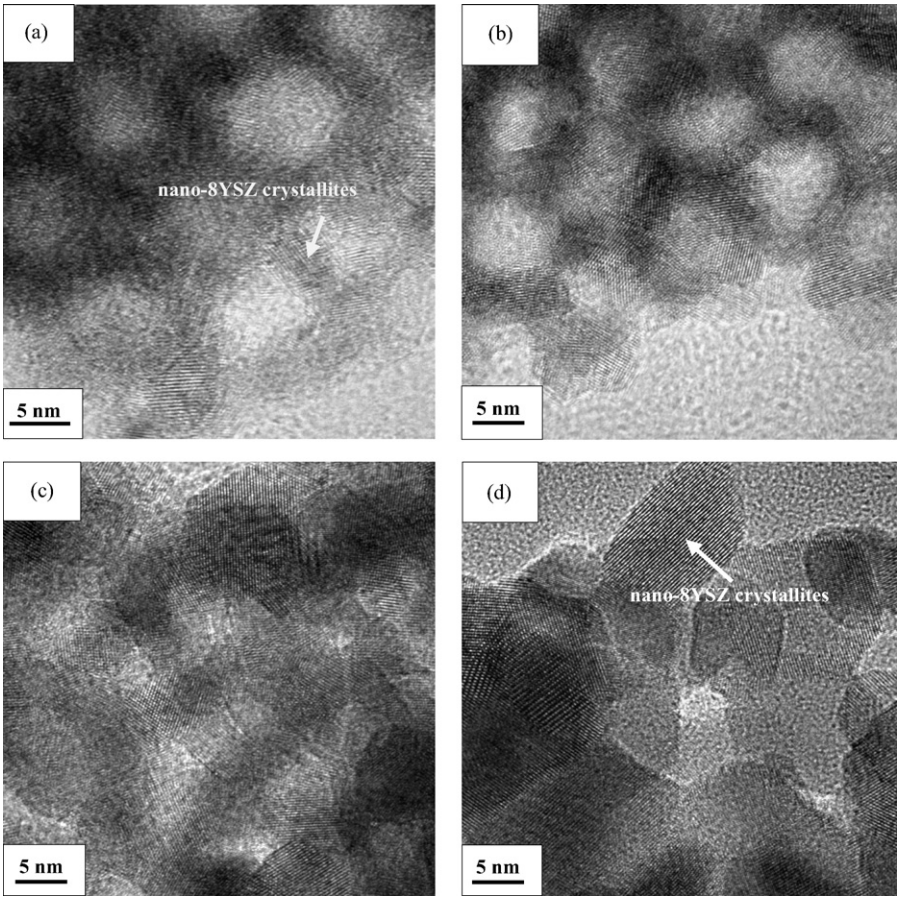

Fig. 6. HR-TEM images of mesoporous nanocrystalline 8YSZ calcined (a) 500 °C, (b) 600 °C (c) 700 °C, and (d) 800 °C for 4 h.

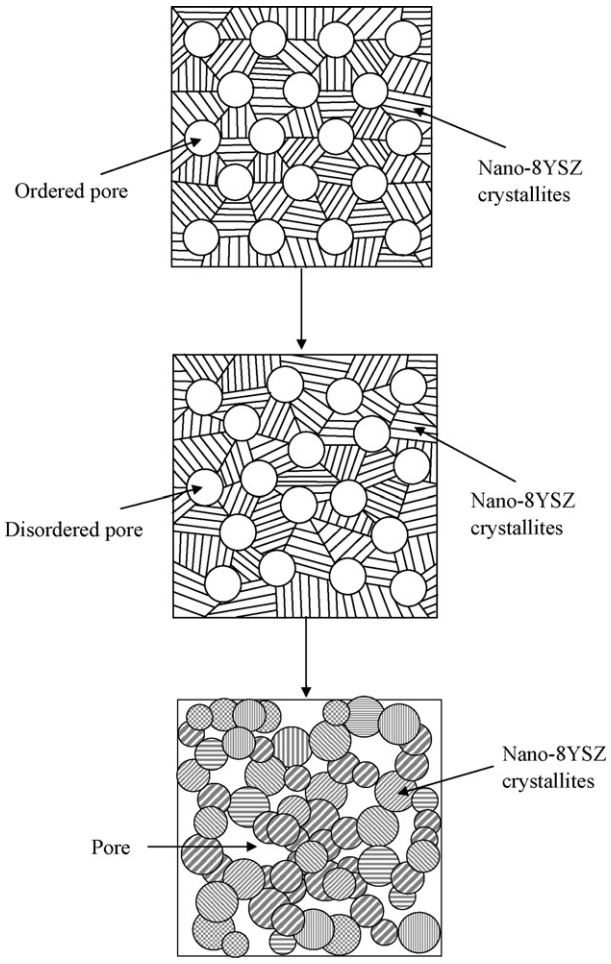

Fig. 7. The schematic diagram for the structure change of mesoporous YSZ during calcination process.

increased to 700 °C; the crystallite size is about 8.3 nm, which is a little larger than the thickness of the pore-walls. However, heating to 800 °C causes the crystallites to grow to approximately 16.6 nm. The growth is likely to be hindered by the wall-pore boundaries. Therefore, it is believed that the degradation of the mesopore ordered arrangement is directly dependencies on the nanocrystalline size. As the crystal size exceeds the thickness of the inorganic wall thickness, the well-ordered mesostructure gradually collapsed. That is why mesoporous silica exhibited better thermal stability than the mesoporous oxides, because the inorganic framework domains in mesoporous silica retain their amorphous structure. The schematic diagrams for the structure change of mesoporous 8YSZ during calcination process are shown in Fig. 7.

From the results described above, the thermal stability of the ordered mesoporous structure may be attributed to the presence of inorganic walls with a thickness of around 6.5 nm. Notably, the main degradation of such an ordered mesoporous structure occurs at the same time as the crystallite growth become larger than the thickness of the inorganic walls. Therefore, the ordered mesoporous structure collapse is directly related to the crystallization and growth of crystallites, which are apt to exceed the geometry of the inorganic framework. It is suggested that the ratio of the thickness of pore-wall to the crystal size of inorganic compound is an important factor to retain the ordered mesostructure at high temperatures.

4. Conclusion

We have presented a highly ordered 2D hexagonal mesoporous 8YSZ based on the EISA method using non-ionic amphiphilic triblock copolymer Pluronic F127 as the templating agent. The thermal stability of the ordered mesoporous structure is related to the crystallite size and the thickness of the inorganic pore-walls. It is demonstrated that as long as the crystallite size of 8YSZ becomes smaller than the thickness of pore-walls, the 8YSZ obtained exhibits very well-ordered mesoporous structure with nanocrystalline pore-walls. On the other hand, as the crystallite size is larger than the thickness of the pore-walls, the ordered arrangement of mesopores collapses.

Acknowledgments

This work is supported by the National Science Council of Taiwan under grant No. NSC-94-2120-M-006-002 and NSC95-2221-E-006-200.

References

1. Kresge, C. T., Leonowicz, M. E., Roth, W. J., Vartuli, J. C. and Beck, J. S., Ordered mesoporous molecular sieves synthesized by a liquid–crystal template mechanism. *Nature*, 1992, **359**, 710–712.
2. Corma, A., From microporous to mesoporous molecular sieve materials and their use in catalysis. *Chem. Rev.*, 1997, **97**, 2373–2420.
3. Ying, J. Y., Mehnert, C. P. and Wong, M. S., Synthesis and applications of supramolecular-templated mesoporous materials. *Angew. Chem. Int. Ed.*, 1999, **38**, 56–77.
4. Schuth, F., Non-siliceous mesostructured and mesoporous materials. *Chem. Mater.*, 2001, **13**, 3184–3195.
5. Coakley, K. M., Liu, Y., McGehee, M. D., Frindell, K. L. and Stucky, G. D., Infiltrating semiconducting polymers into self-assembled mesoporous titania films for photovoltaic applications. *Adv. Funct. Mater.*, 2003, **13**, 301–306.
6. Xu, X., Tian, B., Kong, J., Zhang, S., Liu, B. and Zhao, D., Ordered mesoporous niobium oxide film: a novel matrix for assembling functional proteins for bioelectrochemical applications. *Adv. Mater.*, 2003, **15**, 1932–1936.
7. Peng, Z., Shi, Z. and Liu, M., Mesoporous Sn–TiO_2 composite electrodes for lithium batteries. *Chem. Commun.*, 2000, **21**, 2125–2126.
8. Mamak, M., Coombs, N. and Ozin, G. A., Electroactive mesoporous yttria-stabilized zirconia containing platinum or nickel oxide nanoclusters: a new class of solid oxide fuel cell electrode materials. *Adv. Funct. Mater.*, 2001, **11**, 59–63.
9. Teoh, L. G., Hung, I. M., Shieh, J., Lai, W. H. and Hon, M. H., High sensitivity semiconductor NO_2 gas sensor based on mesoporous WO_3 thin film. *Electrochem. Solid State Lett.*, 2003, **6**, G108–G111.
10. Bagshaw, S. A., Prouzet, E. and Pinnavaia, T. J., Templating of mesoporous molecular sieves by nonionic polyethylene oxide surfactants. *Science*, 1995, **269**, 1242–1244.
11. Selçuk, A. and Atkinson, A., Elastic properties of ceramic oxides used in solid oxide fuel cells (SOFC). *J. Eur. Ceram. Soc.*, 1997, **17**, 1523–1532.
12. Fukui, T., Ohara, S., Naito, M. and Nogi, K., Performance and stability of SOFC anode fabricated from NiO/YSZ composite particles. *J. Eur. Ceram. Soc.*, 2003, **23**, 2963–2967.

13. Can, Z. Y., Narita, H., Mizusaki, J. and Tagawa, H., Detection of carbon monoxide by using zirconia oxygen sensor. *Solid State Ionics*, 1995, **79**, 344–348.
14. Dow, W. P. and Huang, T. J., Effects of oxygen vacancy of yttria-stabilized zirconia support on carbon monoxide oxidation over copper catalyst. *J. Catal.*, 1994, **147**, 322–332.
15. Kim, J. and Lin, Y. S., Sol–gel synthesis and characterization of yttria-stabilized zirconia membranes. *J. Membr. Sci.*, 1998, **139**, 75–83.
16. Mamak, M., Coombs, N. and Ozin, G., Mesoporous yttria-zirconia and metal-yttria-zirconia solid solutions for fuel cells. *Adv. Mater.*, 2000, **12**, 198–202.
17. Chen, F. and Liu, M., Preparation of mesoporous yttria-stabilized zirconia (YSZ) and YSZ–NiO using a triblock copolymer as surfactant. *J. Mater. Chem.*, 2000, **11**, 2603–2605.
18. Wang, Y., Yin, L., Palchik, O., Hacohen, Y. R., Koltypin, Y. and Gedanken, A., Sonochemical synthesis of layered and hexagonal yttrium-zirconium oxides. *Chem. Mater.*, 2001, **13**, 1248–1251.
19. Crepaldi, E. L., Soler-Illia, G. J. de A. A., Bouchara, A., Grosso, D., Durand, D. and Sanchez, C., Controlled formation of highly ordered cubic and hexagonal mesoporous nanocrystalline yttria-zirconia and ceria-zirconia thin films exhibiting high thermal stability. *Angew. Chem. Int. Ed.*, 2003, **42**, 347–351.
20. Brinker, C. J., Lu, Y., Sellinger, A. and Fan, H., Evaporation-induced self-assembly: nanostructures made easy. *Adv. Mater.*, 1999, **11**, 579–585.
21. Cullity, B. D., *Elements of X-ray Diffraction*. Addison-Wesley, California, 1978, pp. 284–285.